ENHANCED PHOTOCATALYTIC DEGRADATION OF NAPHTHALIMIDE-BASED ACID DYES USING Cu/Ag Co-DOPED TiO2 NANOCATALYST OPTIMIZED BY RESPONSE SURFACE METHODOLOGY

*1Amina Muhammad Mustapha, †2Abdulraheem Giwa, ‡2Umar Ameuru Salami and ‡3Eli Danladi

[1]Department of Pure and Applied Chemistry, Faculty of Physical Sciences, College of Computing, Engineering and Science, Kaduna State University, PMB 2339, Kaduna, Nigeria.
[2]Department of Polymer and Textile Engineering, Faculty of Engineering, Ahmadu Bello University, PMB 1500, Zaria, Nigeria.
[3]Department of Physics, Federal University of Health Sciences, PMB 145, Otukpo, Benue State, Nigeria.

*Corresponding authors' email: amina.mustapha@kasu.edu.ng   Phone: +2348038058757
ORCID iD: *https://orcid.org/0000-0002-9164-1406; †https://orcid.org/0000-0001-9783-0411;
‡https://orcid.org/0009-0009-5387-0978; ‡https://orcid.org/0000-0001-5109-4690

ABSTRACT

The environmental persistence and toxicity of synthetic dyes, particularly emerging naphthalimide derivatives, necessitates advanced degradation technologies. This work investigates the photocatalytic degradation of two acid naphthalimide-based dyes using a nanocatalyst synthesized by co-doping TiO2 with Cu/Ag via the co-precipitation technique. The co-doped catalyst exhibited superior properties to pure TiO2, including a reduced crystallite size (28.54 nm), a red-shifted absorption edge (430 nm) corresponding to a narrower bandgap (2.24 eV), and a 61.4% increase in BET surface area (138.77 m^2/g). Process optimization was carried out using response surface methodology (RSM) with a central composite design (CCD) to evaluate the effects of initial dye concentration, pH, catalyst dosage and reaction time. The developed models showed a strong fit ($R^2 > 0.93$) and closely matched the experimental results, achieving high degradation efficiencies of up to 97.31% for Dye A and 97.01% for Dye B. Kinetic modelling revealed that both dyes followed pseudo-first-order kinetics, with rate constants of 0.0331 min^{-1} and 0.0266 min^{-1} and corresponding correlation coefficients ($R^2 = 0.9713$ and 0.9852), indicating surface-limited degradation processes. Substantial mineralization was supported by the Chemical Oxygen Demand (COD) analysis and reductions of 70.0 % and 77.5 % of Dye A and Dye B respectively.

Keywords: Photocatalytic degradation, Cu/Ag co-doped TiO2, Naphthalimide-based acid dyes, Response surface methodology (RSM), Mineralization efficiency

INTRODUCTION

Extensive usage of synthetic dyes in different industries represents a relatively high environmental risk based on the production of a considerable amount of colored waste water (Samsami *et al.*, 2020; Ali *et al.*, 2023). Acid dyes, often based on azo chromophores, are extensively used but frequently exhibit poor exhaustion rates and resistance to conventional treatment, leading to their release into aquatic environments (Lellis *et al.*, 2019). When such dyes persist, they lower the penetration of light and may even have toxic and carcinogenic activities, especially the azo dyes that may degrade to form toxic aromatic amines (Zou and Wang, 2017). Recently, naphthalimide-based dyes have attracted enough attention beyond ordinary dyeing and now have emerging exploitation as advanced functional materials, such as fluorescent chemosensors to detect environmental pollutants or metal ions, cell probes and in biological studies (Shi *et al.*, 2021; Akuma *et al.*, 2025). While valued for their unique photophysical properties and stability in these applications, this inherent stability can translate to environmental persistence if dyes derived from them are released (Shi *et al.*, 2021; Vishani and Shrivastav, 2021). As such, the need to establish efficient ways of degrading these potentially recalcitrant dyes is getting more important.

Conventional wastewater treatment practices are usually incapable of full mineralisation of complex synthetic dyes (Almhana, 2022). The Advanced Oxidation Processes (AOPs), especially the heterogeneous photocatalysis, present a very strong tool that can be used to convert the refractory organic pollutants to simpler inorganic ones (Giovannetti *et al.*, 2017; Mapukata *et al.*, 2023). The choice of the photocatalyst has remained titanium dioxide (TiO2) due to its high efficiency and cost-effectiveness, chemical stability, and non-toxicity, especially against UV light (Saleh *et al.*, 2020; Jiménez-Calvo *et al.*, 2021).

However, the wide band gap energy of TiO2 only absorbs the UV light which makes up just a fraction of the sun's energy (about 4% - 5%) relative to visible light (45%) (Saleh *et al.*, 2020). Furthermore, the high recombination rate of e-/h+ pairs in TiO2 leads to deactivation of the photocatalytic process (Jiménez-Calvo *et al.*, 2021).

In overcoming these shortcomings, considerable efforts are devoted to the synthesis of modified TiO2-based nanocatalysts that could have enhanced visible light and better charge separation efficiency, hence the increased overall degradation of the pollutant (Mao *et al.*, 2024; Chauke *et al.*, 2024). Such factors as particle size, surface area, crystal structure and certain modifications of TiO2 -based catalyst could be the factors influencing its photocatalytic activity significantly (Mapukata *et al.*, 2023; Rajesh *et al.*, 2023).

The empirical performance of photocatalysis is dependent on the optimization of operation parameters since parameters such as initial pollutant concentration, catalyst loading, irradiation conditions and pH of the solution interactively affect the rate of degradation (Rajesh *et al.*, 2023). Response Surface Methodology (RSM) based on experimental designs, such as Central Composite Design (CCD) is one of the powerful statistical methods used to model such complex relationships and determine optimum process conditions in an efficient way. CCD also allows exploring the main and interaction effects of several variables using fewer experiments and, therefore, this is a useful factor to maximize

the efficiency of the photocatalytic degradation processes as it can be seen in different research optimizing the removal of dyes (Batoo *et al.*, 2024; Akuma *et al.*, 2025).

Although there has been a steady increase in the development and use of naphthalimide derivatives in applications such as sensors and imaging (Grabchev *et al.*, 2023), in textile dyeing (Ameuru *et al.*, 2018; Ameuru *et al.*, 2020), and in chemosensors (Shaki *et al.*, 2017) which may see them enter waste streams in greater amounts, the specific research on the degradation of these newer acid dyes using photocatalysis is relatively rare. Existing literature revealed that the photocatalytic degradation of naphthalimide-based acid dyes under statistically optimized reactions conditions is poorly reported. This study thus explores the photocatalytic degradation of naphthalimide-based acid dyes in the presence of a Cu/Ag co-doped TiO$_2$ nanocatalyst under process conditions optimized by Central Composite Design (CCD) to
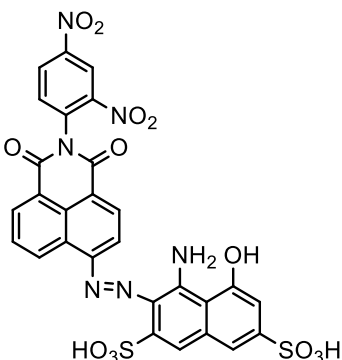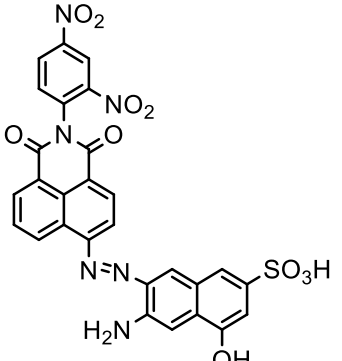
test the degradation efficiency of the system as well as the statistical robustness of the developed models.

MATERIALS AND METHODS
Reagents
All chemicals used in this study were of analytical grade and employed without further purification. Titanium dioxide (TiO$_2$, Changsha Easchem, China), silver nitrate (AgNO$_3$), copper(II)acetatemonohydrate ((CH$_3$COO)$_2$Cu·H$_2$O), sodium hydroxide (NaOH), and hydrochloric acid (HCl) were purchased from Sigma-Aldrich. The dyes studied herein are azo compounds of naphthalimide derivatives that were previously synthesized, structurally confirmed and verified as suitable for application on nylon 6.6 (Mustapha *et al.*, 2025). These dyes are hereafter referred to as Dye A and Dye B, with their molecular structures, IUPAC names, and molecular weights provided in Table 1.

Table 1: Structures of the naphthalimide acid dyes

Dye code	Structure	IUPAC Name	Molecular weight (g/mol)
A		4-amino-3-((2-(2,4-dinitrophenyl)-1,3-dioxo-2,3-dihydro-1H-benzo[de]isoquinolin-6-yl)diazenyl)-5-hydroxynaphthalene-2,7-disulfonic acid	708
B		6-amino-7-((2-(2,4-dinitrophenyl)-1,3-dioxo-2,3-dihydro-1H-benzo[de]isoquinolin-6-yl)diazenyl)-4-hydroxynaphthalene-2-disulfonic acid	628

Synthesis of Cu/Ag titanium oxide co-doped photocatalyst
Cu/Ag co-doped titanium oxide was synthesized by the co-precipitation technique. 0.006M of AgNO$_3$ and Titanium oxide (2 g) with 0.2 M of (CH$_3$COO)$_2$Cu·H$_2$O were combined. Titanium oxide nanoparticles were added to 80 cm^3 deionized water and stirred at 60 °C for 10 min. 5 ml of 0.006 M AgNO$_3$ solution was added gradually to the titanium oxide solution and it was stirred for another 10 min. After that, (CH$_3$COO)$_2$Cu·H$_2$O (20 cm^3) was slowly added under vigorous stirring. The reaction mixture was stirred for a period of 2 hours (500 rpm) at 60 °C and this was followed by the controlled addition of 1 M NaOH (Ph~12), and the mixture was stirred for another 1 hour under the same temperature conditions.

The resulting mixture was filtered, washed repeatedly using distilled water and dried at ambient temperature. The obtained sample was calcined in a furnace at 550 °C for 2 hours to afford Cu/Ag-TiO$_2$ nanocatalyst (Yahya *et al.*, 2023).

Characterization techniques
X-ray diffraction (XRD) and scanning electron microscopy (SEM) were used to determine the structural, textural and morphological properties of the synthesized photocatalyst. Energy Dispersive X-ray (EDX) and BET were used to determine the elemental composition and surface area. The X-ray diffraction (XRD) analysis was done using a Ni-filtered diffractometer coupled with Cu Kα radiation, scanning over a range from 5° to 70° (2θ) at a step interval of 0.5 secs and

Scherrer's equation was used to estimate the crystallite size based on the full width at half maximum (FWHM) of the diffraction peaks (equation 1):

$$D = \frac{K\lambda}{\beta Cos\theta} \tag{1}$$

where D represents the crystallite size (nm), k is the shape factor (0.9), λ is the x-rays wavelength used (0.15406 nm), β is the peak width at half maximum of the diffraction peak in radians, and θ is the Bragg diffraction angle. The morphological features and particle size of the samples were analyzed by Scanning electron microscopy (SEM) equipped with Energy-dispersive X-ray spectroscope (EDS) and surface area analysis was carried out using the Brunauer-Emmett-Teller (BET) method on a Quantachrome NOVA Win instrument (v.11.03).

Photocatalytic experiments

Photocatalytic degradation of Dye A (λmax 546 nm) and Dye B (λmax 545 nm) was carried out in a stirred batch reactor using a 300 W medium-pressure mercury arc lamp positioned 15 cm from the reactor. The spectral irradiance at the reactor surface was 15 ± 2 mW·cm^{-2} at 365 nm, and continuous magnetic stirring maintained a uniform dye-catalyst suspension. pH adjustment was carried out using dilute solutions of HCl and NaOH, depending on the required direction of change. After the reaction time was complete, the samples were passed through a Whatman filter paper No. 1 of 125 mm followed by a microfilter (0.2 μm), and the measurement of the changes in absorbance was conducted using a Perkin Elmer Lambda-25 UV-Visible spectrophotometer. The calibration curve of absorbance vs. concentration of the dyes was constructed to ascertain the linear equations for each dye. The percentage degradation of the dye was determined using the relation in equation (2) (Vaiano and De Marco, 2023):

$$\%\text{Degradation} = \frac{Co - C}{Co} \times 100 \tag{2}$$

where Co and C are the initial and final (after irradiation) dye concentration.

Design of experiments

With the Design Expert software (v13), response surface methodology (RSM) was utilized in the form of Central Composite Design (CCD) to evaluate the role of the process parameters and to optimize the level of the efficiency of dyes A and B photocatalytic degradation with the help of Cu/Ag-doped TiO$_2$. RSM is a powerful method of statistics that is useful in modelling and analysis of relationships between a number of input variables and a response, allowing the generation of the predictive equations that are designed to optimize the process efficiency. Four independent variables were considered in this study: initial dye concentration (5 - 25 ppm), solution pH (2.5 - 6.5), photocatalyst dosage (0.5 - 2.5 g/L) and reaction time (30 - 150 min). Each factor was evaluated at five levels within the experimental domain. A Central Composite Design (CCD) generated 30 experimental runs for each dye, with six replicates at the central point to improve the reliability of error estimation and optimization accuracy. The resulting data were fitted to a quadratic response surface model in order to evaluate both the main effects and the interactions among the independent variables. Table 2 presents the process parameters used in this study.

Kinetic study

Time-course experiments were performed under the optimal conditions identified for each dye. Aliquots were withdrawn every 10 min, immediately isolated from light, clarified to remove suspended catalyst, and analyzed by UV–Vis spectrophotometry at λmax = 546 nm (Dye A) and λmax = 545 nm (Dye B). The concentrations were determined from the calibration curves and two kinetic models were evaluated. For the apparent pseudo-first-order model, the slope of the linear regression of $\ln(C_o/C_t)$ versus time (equation 3) gives k_1 (min^{-1}), and the coefficient of determination (R^2) quantifies the goodness of fit.

$$\ln\left(\frac{Co}{Ct}\right) = k_1 t \tag{3}$$

Where, C_o = initial dye concentration, C_t = concentration of the dye at time t, k_1 = pseudo-first-order rate constant

For the pseudo-second-order model (equation 4), $1/C_t$ was plotted against time and k_2 was obtained from the slope. R^2 was calculated from the same linear regression.

$$\frac{1}{Ct} = \frac{1}{Co} + k_2 t \tag{4}$$

Where, C_o = initial dye concentration, C_t = concentration of the dye at time t, k_2 = pseudo-second-order rate constant.

Determination of Chemical Oxygen Demand (COD)

Closed Reflux Titrimetric Method (APHA, 2017) was applied in determining the Chemical Oxygen Demand (COD). To prepare a sample, 1 ml was diluted to 20 ml with distilled water then 10 ml of standard solution of potassium dichromate (K$_2$Cr$_2$O$_7$) was added together with four glass beads to facilitate uniform boiling. To start the oxidation reaction, 30 ml of concentrated H$_2$SO$_4$ was carefully added which contained Ag$_2$SO$_4$ catalyst and the mixture was refluxed at a regulated temperature for 1 hour in the reaction vessel. After the reflux time, the mixture was cooled and then the condenser was rinsed with distilled water. The obtained solution was later diluted to 100 ml using distilled water. In the titration process, the excess dichromate was titrated against 0.25 N ferrous ammonium sulfate (FAS) solution with 2-3 drops of ferroin indicator and the endpoint was marked as the change in color from blue-green to reddish-brown. The same procedure was followed for a blank determination using distilled water as a baseline that could be used to do calculations. The formula used to calculate the COD value (in mg/L) was established as a baseline for calculations. The COD value (in mg/L) was calculated using the formula:

$$COD \text{ (mg/L)} = \frac{(a-b) \; x \; c \; x \; 8000}{Volume \; of \; sample \; (ml)} \tag{5}$$

Where, a = FAS volume for blank (mL), b = FAS volume for sample (mL), c = Normality of the ferrous ammonium sulfate solution (N) and 8000 = Milliequivalent weight of oxygen × 1000 mL/L.

RESULTS AND DISCUSSION
Catalyst characterization
XRD analysis

Powder XRD analysis was conducted in order to establish the phase structure of both pure and co-doped TiO$_2$. In Figure 1, patterns of X-ray diffraction of TiO$_2$ and Cu/Ag-TiO$_2$ are illustrated. Good level of crystallinity has been recorded in both the samples due to observation of well-sharpened diffraction peaks.
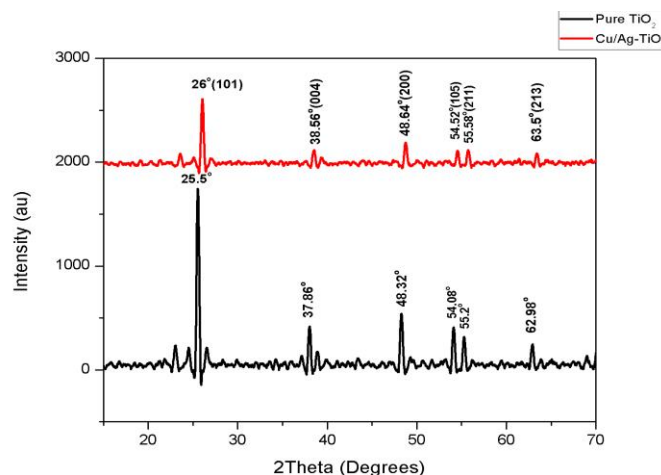
Figure 1: X-ray diffractograms for TiO$_2$ and Cu/Ag-TiO$_2$ nanoparticles

The observed peaks of diffraction are 25.5, 37.86, 48.32, 54.08, 55.2 and 62.98° of the diffraction angle 2θ, which may be identified as (101), (004), (200), (105), (211) and (213) reflections of TiO$_2$, respectively, in the case of pure TiO$_2$. The diffraction peaks at 26.00, 38.56, 48.64, 54.52, 55.58 and 63.50° could be referred to (101), (004), (200), (105), (211) and (213) reflection of TiO$_2$ respectively in the case of co-doped TiO$_2$. The XRD was consistent with the anatase phase of TiO$_2$ (JCPDS Card No. 21-1272). No peak of copper metal or silver was obtained which is evidence that there was no phase change. An interesting finding is however the shift in the peaks in pure TiO$_2$ as compared to Cu/Ag- TiO$_2$ nanoparticles. These changes may suggest lattice strain in the TiO$_2$ structure, which might be due to the incorporation of Cu $^{2+}$ or Ag$^+$ ions into TiO$_2$ lattice demonstrated by the 2 theta values. This observation corroborates the findings of Alqahtani (2024). The size of the crystallites of pure TiO$_2$ and Cu/Ag co-doped TiO$_2$ was determined using the Scherrer equation and the values showed that the size of crystallites in the TiO$_2$ is 34.90 nm and that in Cu/Ag- TiO$_2$ is smaller (28.54 nm). A decrease in the crystallite size could indicate that the process of grain growth in the titania during the synthesis is hindered due to the addition of the dopants which can cause strain and lattice defects and interfere with the tendency of crystallization to occur in an ordered manner. Notably, the

defect states generated by doping may serve as charge traps and extend the lifetime of the photogenerated charge carriers resulting in slowing down the rate of the recombination of the electron hole pairs and hence enhancing the photocatalytic activity (Lee *et al.*, 2021).

UV analysis

The absorbance spectrum of the pure and co-doped TiO$_2$ thinfilm was recorded through UV-Visible absorption spectroscopy and the absorbance band of the pure TiO$_2$ was at 336 nm and in case of the co-doped TiO$_2$ the band has shifted towards the visible region (430 nm). This red shift caused the direct bandgap of the co-doped catalyst to decrease compared with that of pure TiO$_2$ because of the effective incorporation of Cu and Ag into the TiO$_2$ structure which caused a change in its electronic structure. The approximate band gap energy can be calculated using the following equation (5):

$$E = \frac{hc}{\lambda} \qquad\qquad (5)$$

where, h denotes Planck constant, E is the photon energy (band gap), c is the speed of light and λ is wavelength associated with the absorption edge. Figure 2 shows the absorption spectra and the Tauc plot for Cu/Ag-TiO$_2$ nanocatalyst.
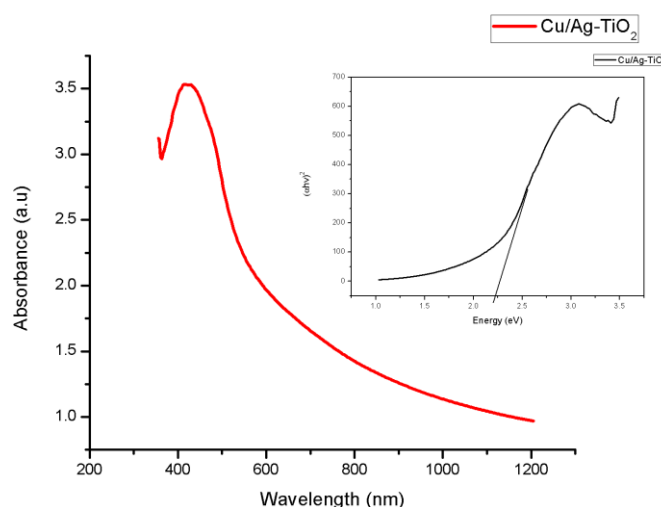
Figure 2: The UV spectrum and Tauc plot for Cu/Ag-TiO$_2$ nanocatalyst

Tauc plot extrapolation revealed a bandgap energy of 2.24 eV for Cu/Ag-TiO$_2$. A red shift leads to a decrease in band gap

energy which consequently results in improvement of light absorption and optical activity of catalyst (Jorfi *et al.*, 2018).

SEM analysis

The morphological properties of the pure TiO_2 sample were observed at different magnifications (1500 x and 5000 x) with the SEM as shown in Figure 3 (a and b). The images were all taken with accelerating voltage of 15kV, working distance of 10.504mm, chamber pressure of 60 Pa and Scale calibration of 10-50 m measurement bars.
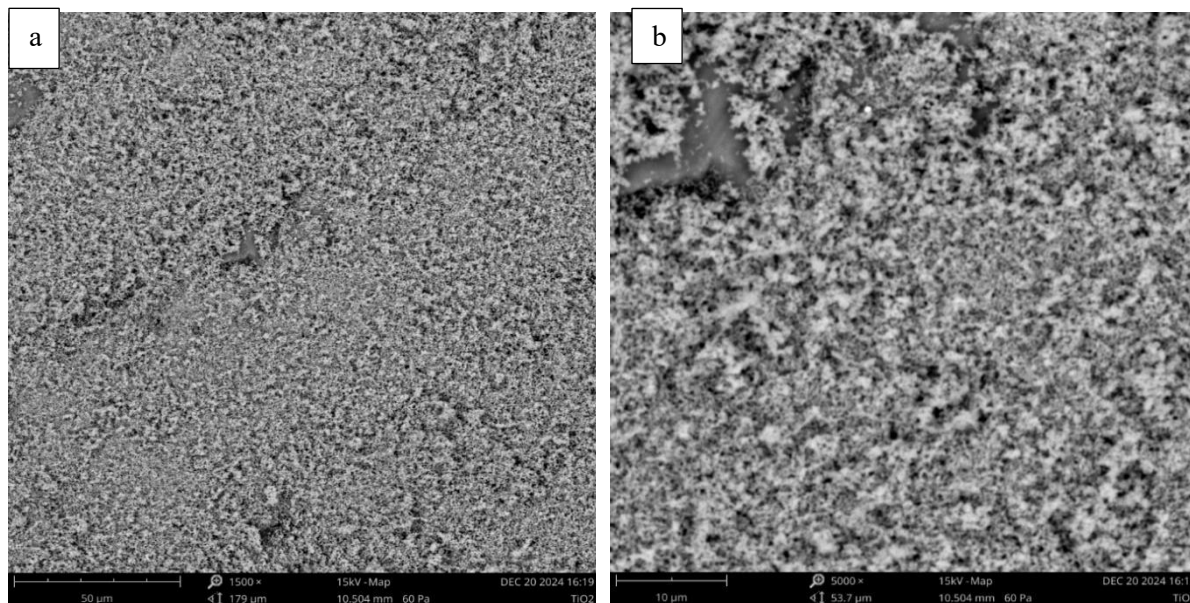

Figure 3: SEM images of pure TiO_2 (a and b)

The main structural characteristics are uniform granular morphology with characteristic TiO_2 nanostructures, hierarchical structure of the particles with multi-scale porosity, high level of interconnectivity between primary particles and lack of large agglomerates that suggest good dispersion. Surface topology shows the homogeneous surface texture at all magnifications, the existence of elaborate networks of inter-particle voids and small grained structure with homogeneous particle distribution and high mesoporosity that is due to dark areas between particles.

The Morphological properties were also observed in the SEM images of Cu/Ag-doped TiO_2 sample at various magnifications (1500x, and 5000x) as depicted in Figure 3 (c and d).
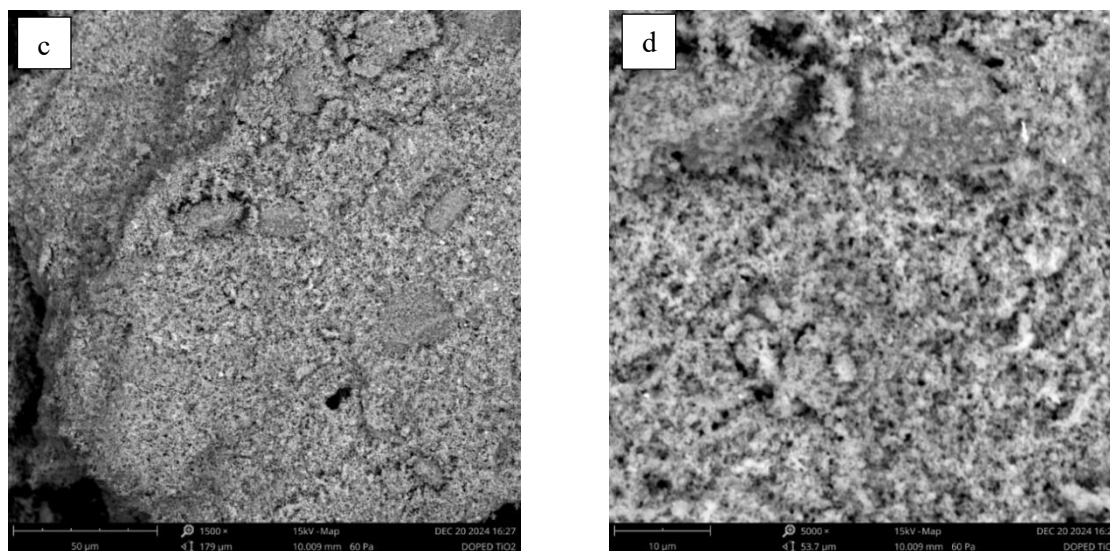

Figure 3: SEM images of Cu/Ag-doped TiO_2 (e, f, g, h)

In the lowest magnification (1500x, Image c), a homogenous and evenly distributed grained structure could be seen with a several distinctive features: the surface has a tendency towards a homogenous distribution of particles, which is an evidence of successful synthesis without serious agglomeration; distinct interconnected porous networks are present, which is advantageous in the process of mass transfer during photocatalytic reaction; the overall texture has a hierarchical structure with both micro and meso-scale features. On higher magnification i.e. 5000x (Image d), better features were found as the network of particles could be seen better, with some intricate connections between the particles; the grain boundaries could be clearly seen between aggregates; differences in size of the pores could be observed, indicating a multi-modal distribution of pores; and also, the roughness of the surface could be realized better, which indicates the effective modification of TiO_2 surface by Cu and Ag.

Energy Dispersive X-ray data of the pure and doped TiO₂
Elemental composition and the actual presence of dopant elements in the synthesized TiO₂ nanoparticles were confirmed using Energy Dispersive X-ray (EDX) spectroscopy. The method supplements the structural and morphological results, by providing quantitative information on the distribution of copper and silver in the synthesized sample as compared with pure TiO₂. Table 2 represents the EDX data of the pure and co-doped materials.

Table 2: The elemental composition of both Pure TiO₂ and Cu/Ag Doped TiO₂

Pure TiO₂				Cu/Ag Doped TiO₂			
Element Number	Element Symbol	Atomic Conc.	Weight Conc.	Element Number	Element Symbol	Atomic Percentage	Weight Percentage
22	Ti	30.46	56.07	22	Ti	27.74	49.56
8	O	67.96	41.81	8	O	65.68	39.22
13	Al	0.82	0.85	29	Cu	3.67	8.71
50	Sn	0.06	0.26	6	C	1.36	0.61
14	Si	0.23	0.25	11	Na	0.70	0.60
38	Sr	0.05	0.18	47	Ag	0.09	0.38
15	P	0.15	0.18	13	Al	0.38	0.38
19	K	0.11	0.17	26	Fe	0.10	0.21
26	Fe	0.07	0.15	14	Si	0.14	0.15
12	Mg	0.07	0.07	19	K	0.05	0.07
20	Ca	0.02	0.03	15	P	0.05	0.06
				20	Ca	0.02	0.04

The EDX analysis confirmed the successful doping of Cu/Ag co-doped TiO₂ sample. The percentages of titanium and oxygen were still dominating at the value of 27.74 and 65.68 respectively that yielded a Ti:O ratio approximately of 1:2.37. This minor overabundance of oxygen could be as a result of hydroxyl groups on the surface of the material which can enhance the formation of the reactive oxygen species, a vital aspect of photocatalytic activity. It is noteworthy that the concentration of the added copper 3.67 atomic percent is close to the level of doping range of 2 - 5 atomic percent, frequently cited as enhancing visible light sensitivity (Slamet *et al.*, 2005). The atomic percent concentration of the silver was found to be 0.09 and is indeed very suitable to act as an efficient plasmonic enhancement without great recombination losses (Gangadhar *et al.*, 2025). A trace of 1.36 atomic percent of carbon was also observed and this can probably be a remnant of the organic precursors during the synthesis process. In some cases, the residual carbon species may also play a part in visible light absorption via extra mid-gap states (Di Valentin *et al.*, 2005). The percentage of Sodium was found as 0.70 which was most likely to have been introduced by sodium hydroxide used in the preparation of the catalyst. The presence of aluminum, silicon, calcium and phosphorus in these samples can be attributed to contamination that originated from the laboratory materials. Collectively, the EDX data confirms the successful incorporation of Cu and Ag dopants.

BET Data of the pure and doped TiO₂
Nitrogen adsorption-desorption isotherm analysis at 77 K was employed to evaluate the surface area, pore volume, and pore size distribution of the synthesized photocatalyst. Specific surface area was determined using Brunauer-Emmett-Teller (BET) method. The mesopore size distribution and the cumulative pore volume was analysed using Barret-Joyner-Halenda (BJH) method on the desorption branch of the isotherm. The micro-pore characteristics were also evaluated with the aid of the Dubinin-Radushkevich (DR) and Dubinin-Astakhov (DA) models which gave information on the pore-heterogeneity and the energy distribution in the material. The results obtained are presented in Table 3.

Table 3: BET Surface area

	BET Data	DA Method		BJH Data				DR Method		Langmuir
Samples	Surface area (m²/g)	Micropore volume (cc/g)	Pore Diameter (mode) (nm)	Surface Area (m²/g)	Pore volume (cc/g)	Pore Diameter Dv(d) (nm)	Average pore width (nm)	Micropore volume (cc/g)	Micropore surface area (m²/g)	Surface area (m²/g)
Pure TiO₂	85.975	0.055	1.82	77.944	0.035	1.453	2.965	0.044	124.042	133.178
Cu/Ag doped TiO₂	138.771	0.126	2.86	170.932	0.083	2.132	5.889	0.056	158.243	480.033
% Increase	61.4	129	57	119	137	46.7	98.6	27.3	27.6	260.4

BET surface area Analysis shows that a major improvement in the specific surface area has taken place upon Cu/Ag co-doping on TiO₂. These results showed a specific surface area of 85.975 m²/g in the pure TiO₂; however, the Cu/ Ag- TiO₂ had a much higher surface area of 138.771 m² /g, which is about a 61.4 percent increase. This significant enhancement in surface area may be associated with addition of Cu and Ag dopants that might have caused changes in the structure of the TiO₂ matrix leading to generation of more surface defects and inability to form agglomerates. In addition, the presence of Cu and Ag ions during synthesis may have altered the crystal growth kinetics, possibly resulting in smaller crystallites or a more porous structure, which may prove advantageous to photocatalytic applications due to increased availability of active sites and ease of mass transfer during photocatalytic reactions (Sapcharoenkun *et al.*, 2025).

The Dubinin-Astakhov (DA) analysis shows that important changes in the pore properties occurred after Cu/Ag co-doping of TiO$_2$. The micropore volume increased significantly by 129 % (0.055 cc/g in pure TiO$_2$ to 0.126 cc/g in Cu/Ag-TiO$_2$). Also, the pore diameter (mode) increased to 2.86 nm in comparison to 1.82 nm. Such a high rise in the micropore volume is consistent with the earlier noticed rise in BET surface area (85.975 to 138.771 m^2 /g). This correlation implies that the co-doping process does not only lead to an increase in the area but also forms more advanced internal pore structure. The increase in micropore volume demonstrates the improvement of the internal porosity that may significantly impact catalytic characteristics of the material. The simultaneous rise in the surface area, micropore volume and the pore diameter indicates a synergetic way of altering the TiO$_2$ structure via Cu/Ag co-doping. This overall structural modification points to the fact that the dopants not merely influence the surface characteristics but also some of the basic alterations in the architectural fabric of the material. Barrett-Joyner-Halenda (BJH) analysis indicates that there is a substantial change in the mesoporous properties of TiO$_2$ after Cu/Ag co-doping. All parameters measured in the analysis indicate high increases in the surface area (77.944 to 170.932 m^2/g), pore volume (0.035 to 0.083 cc/g), and pore diameter (1.453 to 2.132 nm). The BJH data showed an increase in pore volume of 0.035 to 0.083 cc/g (137 %) which is well correlated to the increase in DA micropore volume of 0.055 to 0.126 cc/g. Such a parallel improvement in various analytical procedures implies that Cu/Ag co-doping can be used as an effective way to develop porosity at a wide variety of length scales including micropores and mesopores.

Central Composite Design for the photodegradation of Dye A and Dye B

The influence of different parameters such as catalyst concentration, dye concentration, contact time, and pH on the degradation efficiency of the target pollutants was investigated using RSM-CCD with 30 experiments systematically designed. The process parameters were optimized in order to achieve a maximum photodegradation of both dyes in aqueous solutions. In the design, 0.5 - 2.5 g/L of catalyst, 5 - 25 ppm of dye concentration range, irradiation of the solution for 30-150 min, and the pH range of 2.5 - 6.5 were considered. The Central Composite Design (CCD) matrix along with the experimental results from the photocatalytic degradation studies is presented in Table 4.

Table 4: Experimental matrix of the four-factor Central Composite Design with response values (degradation efficiency (%)) of Dye A and B

Run	Factor 1 A:Conc. (ppm)	Factor 2 B:pH	Factor 3 C:Catalyst dose (g/L)	Factor 4 D:Time (min)	%Degradation (DYE A) Experimental Value	%Degradation (DYE A) Predicted Value	%Degradation (DYE B) Experimental Value	%Degradation (DYE B) Predicted Value
1	15	4.5	0.5	90	91.25	91.35	93	93.98
2	15	4.5	1.5	90	92.32	91.90	94.14	93.67
3	20	5.5	1	60	92.48	91.82	93.67	93.20
4	10	3.5	2	120	92.07	92.43	93.88	93.93
5	10	5.5	1	60	90.33	91.08	92.01	92.10
6	20	5.5	2	120	90.21	90.47	91.86	92.02
7	15	2.5	1.5	90	94.23	94.06	95.92	96.90
8	10	3.5	1	60	95.04	94.48	96.69	96.72
9	20	5.5	1	120	92.2	92.11	93.8	93.60
10	10	5.5	1	120	91.06	90.91	92.71	92.50
11	20	3.5	2	120	90.3	89.98	92.1	91.64
12	25	4.5	1.5	90	96.25	95.87	95.04	95.18
13	5	4.5	1.5	90	97.31	97.57	96	96.36
14	20	3.5	2	60	92.26	92.11	93.91	93.69
15	15	4.5	1.5	90	91.4	91.90	93.05	93.67
16	15	6.5	1.5	90	91.09	91.14	93.12	92.64
17	15	4.5	1.5	90	91.5	91.90	93.7	93.67
18	15	4.5	2.5	90	90.47	90.25	92.12	91.64
19	15	4.5	1.5	30	89.12	89.18	90.72	90.80
20	20	3.5	1	120	91.33	92.05	92.98	93.23
21	15	4.5	1.5	150	87.06	86.88	88.73	89.15
22	15	4.5	1.5	90	92.41	91.90	93.12	93.67
23	10	5.5	2	120	93	93.11	92.49	92.79
24	10	3.5	1	120	91.06	90.66	94.89	93.64
25	20	3.5	1	60	95.1	95.41	97.01	96.31
26	20	5.5	2	60	88.12	88.95	89.72	90.58
27	10	5.5	2	60	93.07	92.05	91.42	91.35
28	15	4.5	1.5	90	92.41	91.90	94.21	93.67
29	15	4.5	1.5	90	91.38	91.90	93.81	93.67
30	10	3.5	2	60	94.5	95.02	96.15	95.98

Model Validation and Comparison with Predictions

Response Surface Methodology (RSM) was able to optimize the following four key parameters of paramount importance namely the concentration of dye, pH, the dose of catalyst and the reaction time. The models that were established were accurate since R^2 exceeded 0.93 as per the calculations of Dye A (R^2 = 0.9568) and Dye B (R^2 = 0.9305). The near similarity between the calculated outcomes and the experiment proves

the strength of the models and the effectiveness of the method of the optimization. In the comparison with the results of Giovannetti *et al.* (2017), the value of R^2 achieved was 0.92, which represents good predictions of the model since the authors used RSM to optimize the photocatalytic processes in degrading organic pollutants as well. Moreover, Dinari and Mahmoudi (2022) utilized the RSM-CCD to optimize the conditions of TiO_2-based photocatalysts under which dyes are degraded to achieve the value R^2 of 0.98 that is quite close to the coefficient of determination (R^2) presented in the current study.

The degradation rates of Dye A (up to 97.31%) and Dye B (up to 97.01%) in the current study are very high implying that Cu/Ag co- doped TiO_2 possess a high catalytic power when using visible light. Comparatively, our findings are slightly above the 95 percent bleaching percentage under visible light of an organic dye, after which Cu-doped TiO_2 nanoparticles were compared in a study by Alqahtani (2024) but very high. This observation agrees with that of our study since the visible

light absorption due to co-doping of TiO_2 with Cu/Ag increased multifold and aided in the quick degradation of the dyes. Similar trend was also observed with Ikram *et al.* (2020) when they employed Cu/Ag-doped TiO_2, because their findings offered degradation efficiencies of more than 90 percent during the degradation of dyes, and also this step goes out to demonstrate the effectiveness of the catalysts in photocatalysis degradation.

Figure 4a and 4b for Dye A and Fig. 4c and 4.d illustrate the performance model of the experimental and predicted values. Figure 4.1a and 4.2a compares the predicted and actual degradation efficiencies for Dye A and Dye B, respectively, showing a close alignment between the two individual set of values. Figure 4b and 4d displays the normal probability plot, where the data points largely follow a straight line with few deviations, indicating a roughly normal distribution. Together, these figures reinforce the strength of the relationship between the model's predictions and the experimental results.
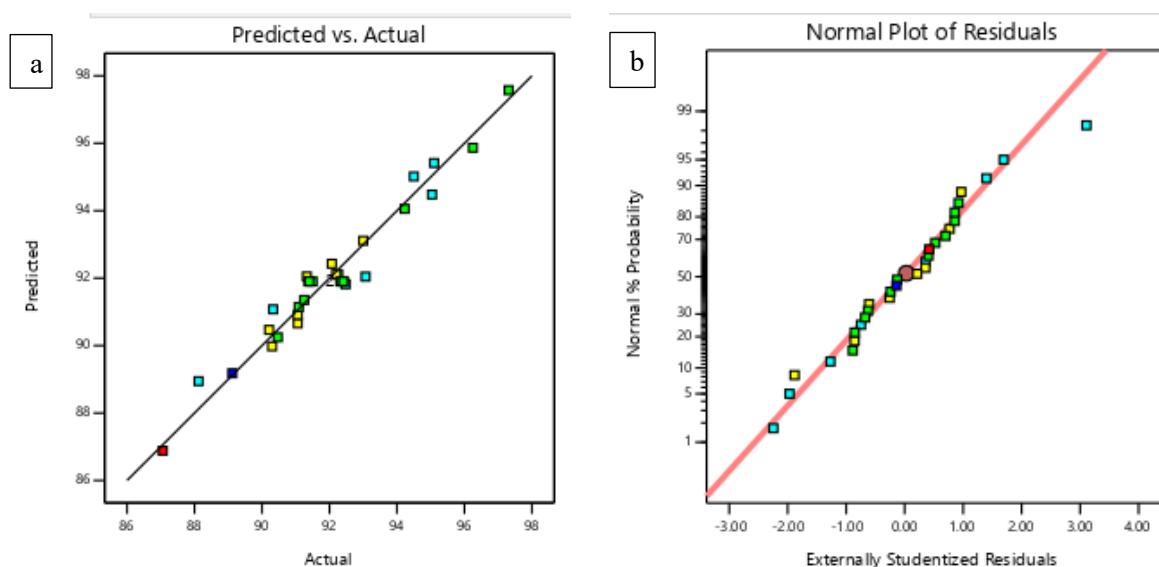

Figure 4: (a) Observed values plotted versus predicted values (b) normal probability plot derived from the photocatalytic degradation of Dye A model
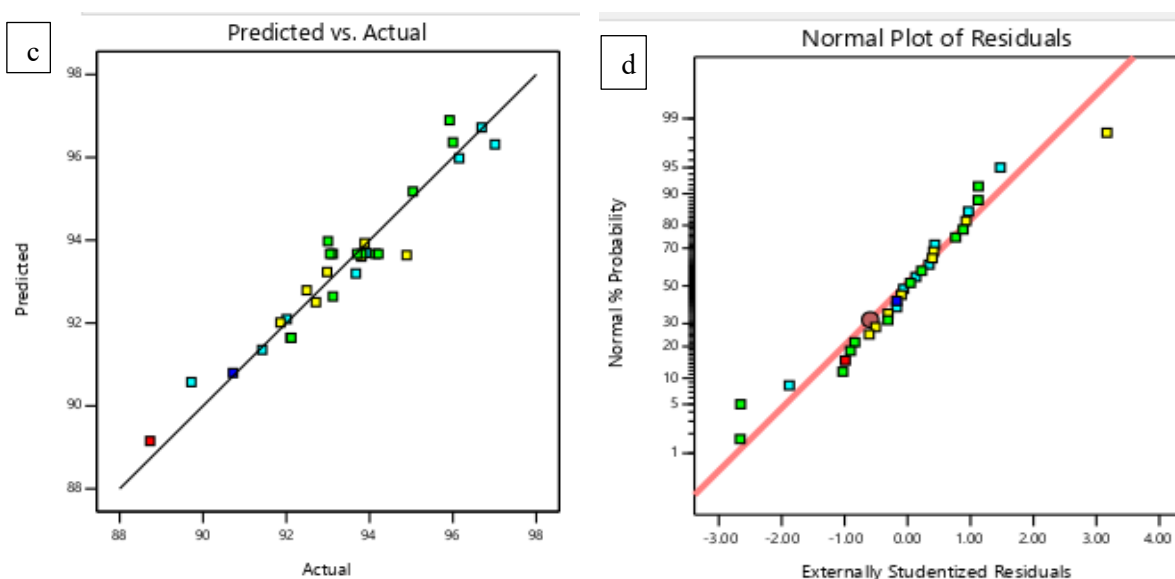

Figure 4 (c) Observed values plotted versus predicted values (d) normal probability plot derived from the photocatalytic degradation of Dye B model

Based on these outcomes, an empirical relationship between the response and independent parameters are expressed by the proposed second-order polynomial equations in Equations 6 and 7 for Dye A (Z_1) and Dye B (Z_2), respectively.

$$Z_1 = -0.4271A - 0.7279B - 0.2762C - 0.576D - 0.0481AB - 0.9606AC + 0.1144AD + 0.1081BC + 0.9131BD + 0.3081CD + 1.2A^2 + 0.1743B^2 - 0.2757C^2 - 0.9682D^2 + 91.9 \tag{6}$$

$$Z_2 = -0.2963A - 0.1.06B - 0.5829C - 0.4104D + 0.3769AB - 0.4694AC + 0.8719BD + 0.2581CD + 0.5245A^2 + 0.2745B^2 - 0.2155C^2 - 0.9243D^2 + 93.67 \tag{7}$$

Analysis of variance

Analysis of variance (ANOVA) was used to obtain the regression coefficients of the second-order terms, the interaction terms and the linear terms. The coefficient of determination (R^2), F-test (Fisher test) and their respective p-values were used to determine whether the models were adequate. The results related to the statistical analysis of variance used to test photodegradation of Dye A and Dye B are given in Table 5a and Table 5b respectively.

Table 5a: Analysis of variance (ANOVA) for the model fitting of degradation efficiency of Dye A based on CCD

Source	Sum of Squares	df	Mean Square	F-value	p-value	
Model	136.66	14	9.76	23.73	< 0.0001	Significant
A-Concentration	4.38	1	4.38	10.64	0.0053	
B-pH	12.72	1	12.72	30.91	< 0.0001	
C-Catalyst dose	1.83	1	1.83	4.45	0.0521	
D-Time	7.92	1	7.92	19.26	0.0005	
AB	0.0371	1	0.0371	0.0901	0.7682	
AC	14.76	1	14.76	35.89	< 0.0001	
AD	0.2093	1	0.2093	0.5087	0.4866	
BC	0.1871	1	0.1871	0.4546	0.5104	
BD	13.34	1	13.34	32.42	< 0.0001	
CD	1.52	1	1.52	3.69	0.0739	
A²	39.78	1	39.78	96.68	< 0.0001	
B²	0.8330	1	0.8330	2.02	0.1752	
C²	2.09	1	2.09	5.07	0.0398	
D²	25.71	1	25.71	62.50	< 0.0001	
Residual	6.17	15	0.4114			
Lack of Fit	4.79	10	0.4795	1.74	0.2809	not significant
Pure Error	1.38	5	0.2754			
Cor Total	142.83	29				

$R^2 = 0.9568$, Adjusted $R^2 = 0.9165$, Predicted $R^2 = 0.7928$

Table 5b: Analysis of variance (ANOVA) for the model fitting of degradation efficiency of Dye B based on CCD

Source	Sum of Squares	df	Mean Square	F-value	p-value	
Model	100.15	12	8.35	18.97	< 0.0001	Significant
A-Concentration	2.11	1	2.11	4.79	0.0429	
B-pH	27.16	1	27.16	61.74	< 0.0001	
C-Catalyst dose	8.16	1	8.16	18.54	0.0005	
D-Time	4.04	1	4.04	9.19	0.0075	
AB	2.27	1	2.27	5.17	0.0363	
AC	3.53	1	3.53	8.01	0.0115	
BD	12.16	1	12.16	27.65	< 0.0001	
CD	1.07	1	1.07	2.42	0.1379	
A²	7.55	1	7.55	17.15	0.0007	
B²	2.07	1	2.07	4.70	0.0447	
C²	1.27	1	1.27	2.90	0.1070	
D²	23.43	1	23.43	53.27	< 0.0001	
Residual	7.48	17	0.4399			
Lack of Fit	6.26	12	0.5215	2.14	0.2069	not significant
Pure Error	1.22	5	0.2440			
Cor Total	107.63	29				

$R^2 = 0.9305$, Adjusted $R^2 = 0.8815$, Predicted $R^2 = 0.7266$

R^2 indicates the good fit of the model to the data as values that are close to 1.0 show a high relationship between the results that are closely observed and those that are estimated by the model. In Dye A, the R^2 and R^2 adj are 0.9568 and 0.9165 respectively while for Dye B it is 0.9305 and 0.8815 respectively and this proves that the model is a good representation of the experimental results. Statistical analysis of the significance of developed models was done through F-test and p-values. In order to further prove the validity of our models, Analysis of Variance (ANOVA) was used, which shows the significance of main factors - pH, dye concentration and catalyst dosage, and also their interactions. These findings showed that all important determinants significantly affected the degradation process since the p-values were well below

the 0.05 level, which proves the importance of these parameters in our model. Moreover, the insignificance of the lack of fit of the models supported the appropriateness of experimental conditions and stability of the models because they would properly reflect the observed data.

In our study, the statistical results are consistent with the research conducted by Batoo *et al.* (2024) who worked on optimizing the process of photocatalytic degradation of tetracycline by utilizing RSM and CCD and validated their model via ANOVA. The p-values reported on the important factors were also significant, which was the same in our case in terms of the experimental parameters.

Also, to achieve a good design space in RSM, the value of precision needs to be adequate, i.e., greater than 4, since the

value indicates that the model contains a large signal to noise ratio to cover the design space (Dinari and Mahmoudi, 2022). The values of adequate precision were determined to be 23.58 and 17.74 respectively which both surpassed the acceptable value of 4 hence indicating that the two models have an adequate signal to noise ratio. Furthermore, the values of coefficient of variations are low, 0.6971 for Dye A and 0.7101 for Dye B, which further holds in the reliability and reproducibility of the developed models.

Interaction effects of operational parameters

The plots of the 3D response surface in Figures 5a, b, c and d indicate the interactions between the main effects on the degradation efficiencies of Dye A.
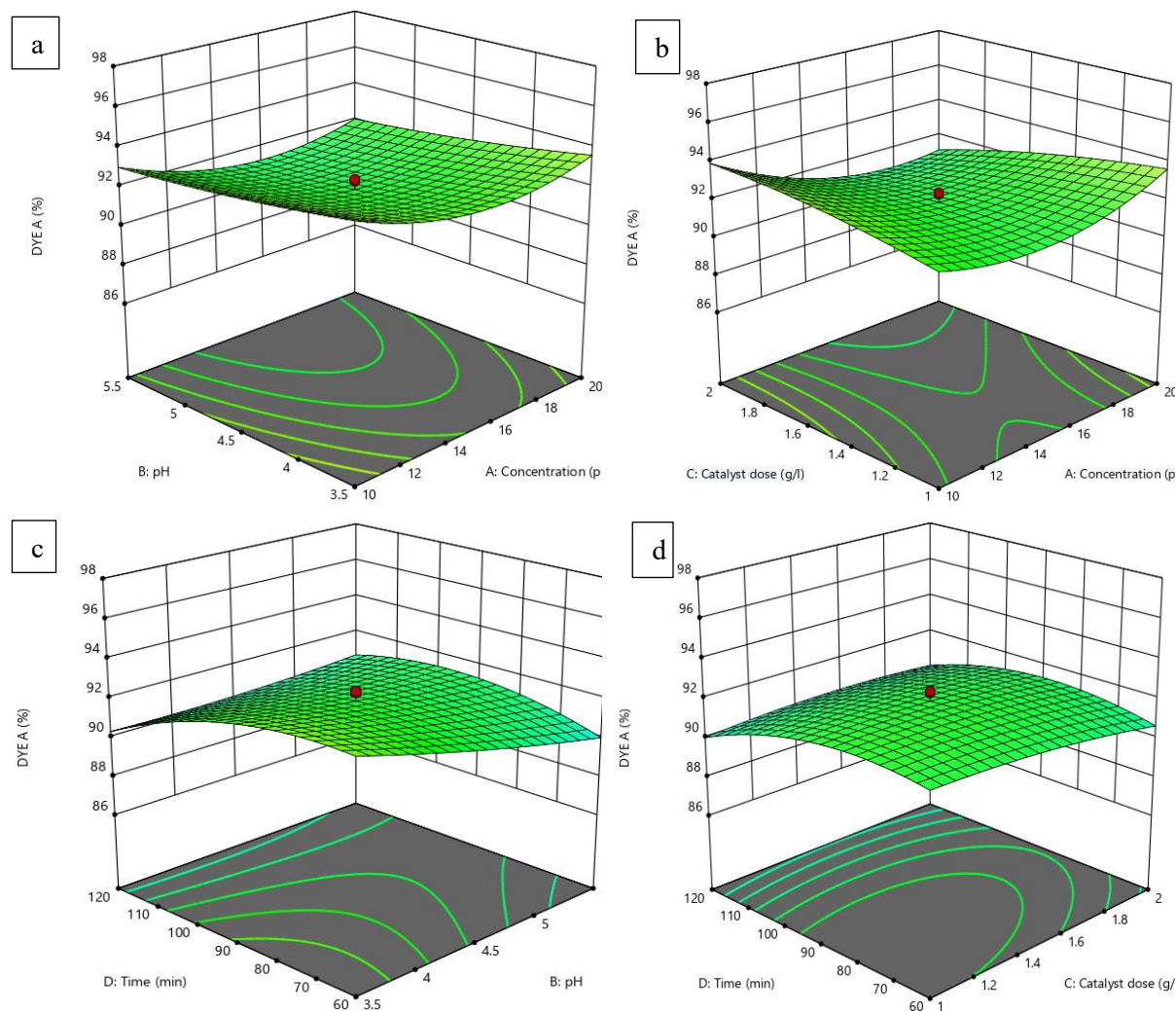

Figure 5: Three-Dimensional response surface and corresponding contour plots showing the effects of (a) pH and initial dye concentration (b) catalyst dose and initial dye concentration (c) Time and pH (d) Time and catalyst dose, on the degradation efficiency (%) of Dye A

The quadratic CCD model described the Dye A response well ($R^2 = 0.9568$; adjusted $R^2 = 0.9165$; predicted $R^2 = 0.7928$). Lack-of-fit was not significant (p = 0.2809), and the overall model was significant (p < 0.0001). Among main effects, pH and irradiation time were strong (p < 0.0001 and p = 0.0005), dye concentration was significant (p = 0.0053), and catalyst dose was marginal (p = 0.0521). Significant quadratic terms in A^2, C^2 and D^2 indicate that the maximum performance lies within the tested ranges. Of the interactions, AC (concentration x dose) and BD (time x pH) were significant

(both p < 0.0001), while AB, AD, BC, CD were not (p > 0.05). The four response - surface plots cover the central region A (10 - 20 ppm), B (3.5 - 5.5), C (1.0 - 2.0 g L^{-1}) and D (60 - 120 min).

Degradation efficiency increases toward the upper end of the tested pH range, while concentration shows a shallow curvature; in the B - A surface, values above ~92% occur at pH ~5.0 - 5.5 with A ~15 - 20 ppm, whereas a softer region appears near pH ~4.0 - 4.5 and A ~12 - 14 ppm (~90%). Because AB is not significant (p = 0.7682), these trends

reflect largely independent effects of pH and concentration. By contrast, AC is significant ($p < 0.0001$): the benefit of increasing catalyst dose depends on concentration. At low to moderate A, raising C increases degradation efficiency by providing more accessible catalytic surface; at higher A, the extra gain is small because the dye absorbs part of the incident light (inner-filter effect) and a denser suspension scatters light, so fewer photons reach the particles. In the C - A surface, the high-response region is A ~16 - 20 ppm with C ~1.6 - 2.0 g L^{-1} (about 92 - 94%), while C ≤ 1.2 g L^{-1} with A ~12 - 14 ppm yields ~88 - 90%. This interaction and the presence of an optimal TiO$_2$ loading are consistent with prior slurry-reactor studies that attribute plateaus at high concentration or loading to optical limitations. (Reza *et al.*, 2015; Tolosana-Moranchel *et al.*, 2020).

The BD interaction is significant ($p < 0.0001$). Extending irradiation is most effective toward the upper part of the tested pH range. In the D - B surface, degradation peaks around pH ~4.6 - 5.0 at ~95 - 105 min (≈93 - 94%) and then levels off. Beyond ~110 - 115 min additional time yields little benefit. The CD interaction is not significant ($p = 0.0739$), although the significant C^2 and D^2 terms produce curvature in both factors. In the D - C surface, time and catalyst dose act largely additively. Performance improves up to about C ~1.3 - 1.6 g L^{-1} and D ~90 - 105 min, then plateaus. Pushing to C ≈ 2.0 g L^{-1} or D ≥ 115 min does not increase efficiency and can edge it down toward ~90%, which is consistent with limited photon delivery in more opaque slurries. These patterns align with reports of irradiation plateaus and optical constraints in TiO$_2$ slurry reactors, where further exposure gives diminishing returns once photon flux at the catalyst surface becomes limiting (Tran *et al.*, 2023, Tolosana-Moranchel *et al.*, 2020). The plots of the 3D response surface in Figures 6a, b, c and d indicate the interactions between the main effects on the degradation efficiencies of Dye B.
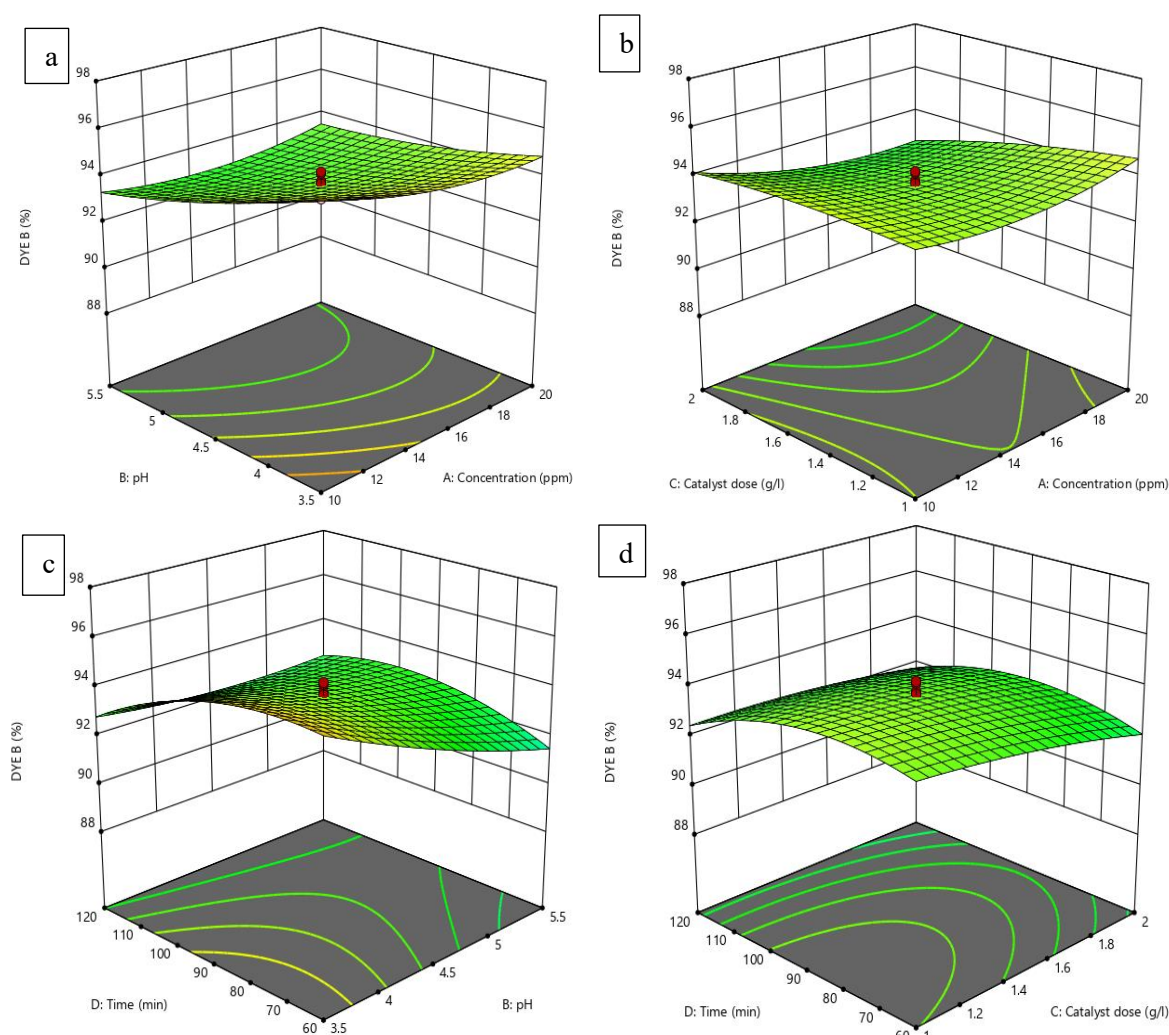

Figure 6: Three-Dimensional response surface and corresponding contour plots showing the effects of (a) pH and initial dye concentration (b) catalyst dose and initial dye concentration (c) Time and pH (d) Time and catalyst dose, on the degradation efficiency (%) of Dye A

The quadratic CCD model explained the Dye B response well ($R^2 = 0.9305$, adjusted $R^2 = 0.8815$, predicted $R^2 = 0.7266$). Lack of fit was not significant ($p = 0.2069$) and the overall model was significant ($p < 0.0001$). Among the main effects, pH was very strong (B, $p < 0.0001$), catalyst dose was strong (C, $p = 0.0005$), irradiation time was significant (D, $p =$ 0.0075), and concentration had a smaller but real effect (A, $p = 0.0429$). Curvature was present in A^2 ($p = 0.0007$), B^2 ($p = 0.0447$), and D^2 ($p < 0.0001$), while C^2 was not significant ($p = 0.1070$), which suggests bending toward an interior optimum with respect to concentration, pH, and time across the explored space. This pattern and the choice of CCD - RSM

agree with earlier TiO_2 photocatalysis studies that used RSM to capture curvature and interactions among pH, concentration, dose, and time (Mortazavian *et al.*, 2019).

The pH - concentration surface shows a real interaction (AB, p = 0.0363). Degradation increases as pH moves to the upper part of the tested window, while concentration shows mild curvature. From the plot, values above about 92% occur for pH around 5.0 to 5.5 with concentration around 16 to 20 ppm, whereas a weaker region appears near pH about 3.8 to 4.3 with concentration around 11 to 13 ppm, where the surface is near 89 to 90%. This pH trend is consistent with reports that pH controls dye speciation and TiO_2 surface charge and that mildly acidic to near-neutral conditions often favor photodegradation of acid and azo dyes (Reza, 2017). The concentration - dose surface also shows a significant interaction (AC, p = 0.0115). Increasing dose is productive at low to moderate concentration, but the gain becomes small at higher concentration because the dye absorbs more of the incident light and a denser suspension scatters it, so fewer photons reach the catalyst. In the plot, the high-response region is concentration about 16 to 20 ppm with dose about 1.6 to 2.0 g L^{-1} (roughly 92 to 94%), while dose at or below 1.2 g L^{-1} with concentration around 12 to 14 ppm yields about 88 to 90%. The existence of an optimal loading and the inner-filter and scattering limits are well documented for TiO_2 slurries (Reza *et al.*, 2015).

Time interacts strongly with pH (BD, p < 0.0001) and not with dose (CD, p = 0.1379), although time shows clear curvature through D^2. On the time - pH surface, efficiency climbs to a peak around pH 4.6 to 5.0 at about 90 to 100 minutes, then levels off such that extending irradiation beyond about 105 to 110 minutes adds only a little impact. Such plateaus are widely reported once photon supply or surface sites become limiting and they match pseudo-order kinetic behavior observed in photocatalytic systems (Tran *et al.*, 2023). On the time - dose surface, time and dose act largely additively. Performance improves up to about 1.3 to 1.6 g L^{-1} and 90 to 105 minutes, then approaches a plateau, and pushing dose toward 2.0 g L^{-1} or time to 120 minutes does not raise the surface further, which is consistent with optical limits in more opaque suspensions (Tolosana-Moranchel *et al.*, 2020). Taken together, a practical window for Dye B is pH about 5.0 to 5.5, concentration about 16 to 20 ppm, catalyst dose about 1.6 to 2.0 g L^{-1} at the upper concentration band or 1.3 to 1.6 g L^{-1} at moderate concentration, and irradiation time about 90 to 105 minutes.

Mechanistic Insights and Kinetic Modelling

Kinetics of photocatalytic degradation is the key to not only assessing the efficiency of the reaction, but also determining mechanistic pathway and the rate-limiting steps. The degradation kinetics of Dye A and Dye B were both fit by pseudo-first-order and pseudo-second-order methods, and the findings was utilized in elucidating the kinetics of surface interactions and the dynamics of the reactive species involved in the photocatalytic reaction. The degradation of dye A was done using the optimum conditions of 5 ppm initial concentration, pH 4.5, 1.5 g/L catalyst dose and 90 minutes UV irradiation. UV-visible spectrophotometry was utilized to measure concentration at 10-minute intervals and the kinetic data were fitted to pseudo-first-order and pseudo-second-order models.

The pseudo-first-order model where the change of $\ln(C_o/C_t)$ with time is expressed linearly, gave a rate constant $k_1 = 0.0331$ min^{-1} and a coefficient of determination $R^2 = 0.9713$ implying a very good fit. On the other hand, the pseudo-second-order model had a weak fit with $R^2 = 0.6814$, thus, supporting the first-order model. Such behaviour is typical of some photocatalytic systems that are used at low dye concentrations, with surface-active sites present in excess to the adsorbed molecules (Gaya and Abdullah, 2008). Similar results were presented by Chauke *et al.* (2024), who found that TiO_2-based photocatalysts could be described under first-order kinetics since the number of accessible active sites interacting with dye and radicals produced by photons was significant. Therefore, the degradation rate is mainly controlled by adsorption of dye molecules, and the reaction of these adsorbed molecules with photo-generated radicals at the catalyst surface.

In Dye B, the optimum degradation conditions were 20 ppm dye concentration, pH 3.5, 1.0 g/L dose of catalyst and 60 minutes exposure to UV irradiation. The results of the concentration-time analysis showed that the concentration of the dye decreased very quickly with the end result being more than 97 percent degradation under acidic conditions. The kinetic modelling provided a value of pseudo-first-order rate parameter $k_1 = 0.0266$ min^{-1} and $R^2 = 0.9852$, which are strongly consistent with the model once again. The pseudo second order fit, in comparison, was much weaker ($R^2 = 0.7816$), confirming the dominance of first-order kinetics. Such a similarity in both dyes favors the concept that the Cu/Ag co-doped TiO_2 catalyst is mostly surface-limited and involved in the interaction of dye molecules with photo-generated radicals absorbed on the catalyst surface (Samsami *et al.*, 2020; Lee *et al.*, 2021). The pseudo-first-order plot for Dye A and Dye B are depicted in Figure 7.
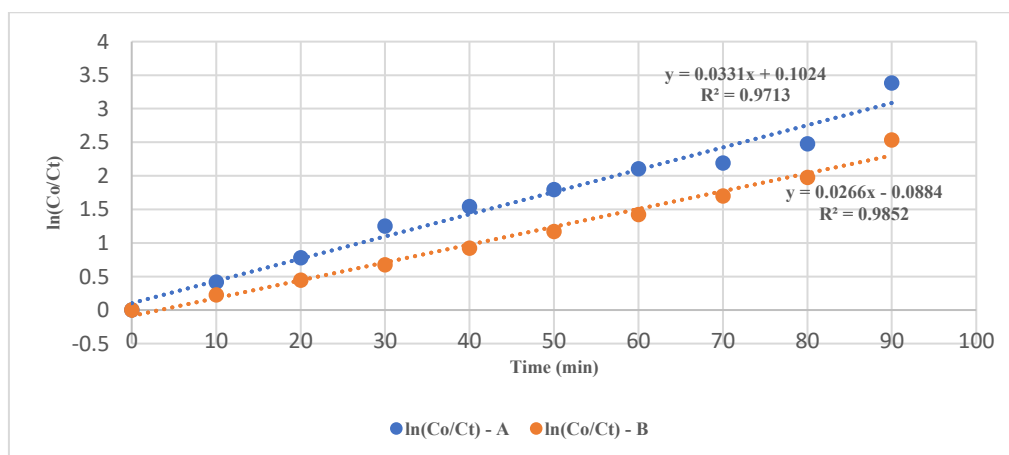

Figure 7: Pseudo-first-order plot ($\ln(C_o/C_t)$ vs. time) for Dye A and Dye B

Mineralization of Dye A and Dye B

Mineralization of Dye A and Dye B through photo-degradation reaction was determined via COD analysis under conditions of 20 mg/L initial dye concentration, pH 3.5, 1.5 g/L photocatalyst dosage and 90 minutes reaction time. The COD was evaluated before and after photodegradation experiment for both dyes, and these results are summarized in Table 6.

$$Mineralization\ (\%) = \frac{COD_i - COD_f}{COD_i} \times 100 \qquad (8)$$

where, COD_i and COD_f are COD concentrations at beginning of the reaction and at time t

Table 6: Chemical Oxygen Demand (COD) Reduction for Dyes after Photocatalytic Treatment

Dye Sample	Initial COD (mg/L)	Final COD (mg/L)	Absolute Reduction (mg/L)	Percentage Reduction (%)
DYE A	400	120	280	70.0
DYE B	400	90	310	77.5

An important index of water quality is Chemical Oxygen Demand (COD) which is the total amount of the oxygen needed to oxidize the organic pollutants. The initial COD of both the dye solutions that is, Dye A and Dye B were 400mg/L. This high quantity of COD means that the naphthalimide-based dye was highly contaminated with organic compounds which require so much oxygen to oxidize. The COD of degraded solutions of Dye A and Dye B reduced to 120 mg/L and 90 mg/L respectively. The substantial COD reductions obtained indicate that the photocatalytic degradation process employing the Cu/Ag co-doped TiO_2 nanocatalyst was effective in oxidizing and degrading a significant portion of the organic structure of these complex naphthalimide-derived acid dyes. This level of mineralization is a critical outcome, signifying a more complete and environmentally sound treatment approach compared to processes that only achieve decolorization.

Limitations and Recommendations

This research was on the degradation process of two dyes that were based on naphthalimide in a standardized aqueous medium, and the results may not depict accurately real-life conditions of effluents, which can have multiple pollutants and differing pH levels. The Cu/Ag co-doped TiO_2 nanocatalyst also was not exhausted in performance testing with respect to long-term stability as well as metal leaching. Besides, there was no assessment of the effect of the treated effluent on the environment. These limitations can be overcome in future studies through the testing of the catalyst in complex effluents, in addition to investigating the catalyst under natural sunlight, as well as evaluating how durable it is in multiple cycles. Mechanistic research is also advised in order to ascertain the reaction pathways and enhance the rate of mineralization. To show a better picture of the scalability and practicality of the catalyst, a techno-economic assessment and environmental life-cycle analysis would be of importance.

Implications/Future perspectives

The results of the current research have revealed the possibility of Cu/Ag co-doped TiO_2 as a potential photocatalyst to degrade azo dyes, which hold much hope in industrial wastewater treatment. Its favourable degradation efficiency (up to 97%) and large mineralization (COD reductions of up to 77.5%) imply that this catalyst might be used to treat dye-bearing effluents, particularly in those industries where effluent treatment is a serious concern like textiles industries. Optimization of important parameters like pH, dosage of catalyst and contact time will be a guide on the practical use of the same in the real-world scenario where slight change in the process conditions can result in better treatment. Also, the visible light sensitivity of the catalyst may lower the energy expenditure and make the catalyst more viable at an industrial scale. Such a strategy is able to not only help resolve the significant environmental issue, but can bring the possibility of fitting photocatalytic procedures into already established wastewater treatment facilities to the table, which are more sustainable and energy efficient.

CONCLUSION

This study demonstrated the photocatalytic potential of the synthesized Cu/Ag co-doped TiO_2 nanocatalyst in the degradation of some azo acid dyes based on naphthalimide derivatives. The combination of structural and optical properties was superior to undoped TiO_2 as the co-doped catalyst had a higher surface area, enhanced porosity and better visible light absorption due to which it had high photocatalytic activity under visible light irradiation. The Response Surface Methodology based on Central Composite Design effectively enhanced parameter optimization which resulted in high degradation efficiencies (up to 97.31 % in the case of Dye A and up to 97.01 % in the case of Dye B). The fact that there was significant mineralization was supported by a significant reduction in the Chemical Oxygen Demand (70.0 % and 77.5 % of the initial value in Dye A and B respectively). The study helps to address an important gap in the literature because it involves a systematic study of the photocatalytic degradation of these persistent naphthalimide-based acid dyes and their optimization. The results indicate the viability of the Cu/Ag-TiO_2 nanocatalyst as a remedy to the problem of treating wastewater polluted by such recalcitrant pollutants. The aim of further research can be the complete mineralization and the investigation of pilot-scale activities.

REFERENCES

Akuma, D. A., Lund, H., Duong, T. T. H., Fufa, F., Strunk, J., & Steinfeldt, N. (2025). Optimization of Anatase TiO_2 photocatalyst for diclofenac degradation by using response surface methodology. *Applied Sciences*, *15*(3), 1401. https://doi.org/10.3390/app15031401

Ali, A. E., Chowdhury, Z. Z., Devnath, R., Ahmed, M. M., Rahman, M. M., Khalid, K., Wahab, Y. A., Badruddin, I. A., Kamangar, S., Hussien, M., Pallan, K. H., & Mitra, A. (2023). Removal of Azo Dyes from Aqueous Effluent Using Bio-Based Activated Carbons: Toxicity Aspects and Environmental Impact. *Separations*, *10*(9), 506. https://doi.org/10.3390/separations10090506

Almhana, N., Naser, Z., Najjar, S. A., Al-Sharify, Z., & Nail, T. (2022). Photocatalytic Degradation of Textile Dye from Wastewater by using ZnS/TiO_2 Nanocomposites Material. *Egyptian Journal of Chemistry*, *0*(0), 0. https://doi.org/10.21608/ejchem.2022.125852.5588

Alqahtani, F. O. (2024). Advancing photocatalytic degradation under visible light with TiO$_2$/g-C$_3$N$_4$ nanohybrid mechanistic insights. *Journal of Saudi Chemical Society*, *28*(5), 101918. https://doi.org/10.1016/j.jscs.2024.101918

American Public Health Association (APHA) (2017) Standard methods for the examination of water and wastewater. 23rd edn. American Public Health Association, American Water Works Association, Water Environment Federation, Washington, DC.

Ameuru, U. S., Yakubu, M. K., Bello, K. A., Nkeonye, P. O., & Halimehjani, A. Z. (2018). Synthesis of disperse dyes derived from 4-amino-N-decyl-1, 8-naphthalimide and their dyeing properties on polyester fabrics. *Dyes and Pigments*, *157*, 190-197. https://doi.org/10.1016/j.dyepig.2018.04.050

Ameuru, U., Yakubu, M., Bello, K., Nkeonye, P., & Halimehjani, A. (2020). Synthesis and dyeing performance of some amphiphilic naphthalimide azo disperse dyes on polyester fabrics. *Journal of the Serbian Chemical Society*, *85*(10), 1253-1264. https://doi.org/10.2298/jsc190123049a

Anwer, H., Mahmood, A., Lee, J., Kim, K., Park, J., & Yip, A. C. K. (2019). Photocatalysts for degradation of dyes in industrial effluents: Opportunities and challenges. *Nano Research*, *12*(5), 955-972. https://doi.org/10.1007/s12274-019-2287-0

Batoo, K. M., Jassim, K. H., Qassem, T. A., Hussain, S., Hasson, W. T., Jalal, S. S., Ramadan, M. F., Hameed, S. M., Alawadi, A. H., & Alsaalamy, A. (2024). Novel magnetically separable g-C$_3$N$_4$/ TiO$_2$/CuFe$_2$O$_4$ photocatalyst for efficient degradation of tetracycline under visible light irradiation: Optimization of process by RSM. *Journal of Saudi Chemical Society*, *28*(3), 101871. https://doi.org/10.1016/j.jscs.2024.101871

Chauke, N. M., Mohlala, R. L., Ngqoloda, S., & Raphulu, M. C. (2024). Harnessing visible light: enhancing TiO$_2$ photocatalysis with photosensitizers for sustainable and efficient environmental solutions. *Frontiers in Chemical Engineering*, *6*. https://doi.org/10.3389/fceng.2024.1356021

Di Valentin, C., Pacchioni, G., & Selloni, A. (2005). Theory of carbon doping of titanium dioxide. *Chemistry of Materials*, *17*(26), 6656-6665. https://doi.org/10.1021/cm051921h

Dinari, A., Mahmoudi, J., & School of Chemistry, Damghan University, Damghan, Iran. (n.d.). Response surface methodology analysis of the photodegradation of methyl orange dye using synthesized TiO$_2$/Bentonite/ZnO composites. *Advances in Environmental Technology*, *1*, 31-46. https://doi.org/10.22104/AET.2022.5204.1409

Gangadhar, T. G., Kumar, M. V. P., Thimmaiah, M. B., Jagadeesha, T., Math, M. M., & Saravanakumar, G. (2025). Photocatalytic performance of silver-doped titanium dioxide (TiO$_2$) nanoparticles for environmental applications. *Materials Technology*, *40*(1). https://doi.org/10.1080/10667857.2025.2502960

Garcia-Segura, S., & Brillas, E. (2017). Applied photoelectrocatalysis on the degradation of organic pollutants in wastewaters. *Journal of Photochemistry and Photobiology C Photochemistry Reviews*, *31*, 1-35. https://doi.org/10.1016/j.jphotochemrev.2017.01.005

Gaya, U. I., & Abdullah, A. H. (2008). Heterogeneous photocatalytic degradation of organic contaminants over titanium dioxide: A review of fundamentals, progress and problems. *Journal of Photochemistry and Photobiology C Photochemistry Reviews*, *9*(1), 1-12. https://doi.org/10.1016/j.jphotochemrev.2007.12.003

Giovannetti, R., Rommozzi, E., Zannotti, M., & D'Amato, C. A. (2017). Recent advances in graphene based TIO2 nanocomposites (GTiO$_2$Ns) for photocatalytic degradation of synthetic dyes. *Catalysts*, *7*(10), 305. https://doi.org/10.3390/catal7100305

Grabchev, I., Angelova, S., & Staneva, D. (2023). Yellow-Green and Blue fluorescent 1,8-Naphthalimide-Based chemosensors for metal cations. *Inorganics*, *11*(2), 47. https://doi.org/10.3390/inorganics11020047

Ikram, M., Umar, E., Raza, A., Haider, A., Naz, S., Ul-Hamid, A., Haider, J., Shahzadi, I., Hassan, J., & Ali, S. (2020). Dye degradation performance, bactericidal behavior and molecular docking analysis of Cu-doped TiO$_2$ nanoparticles. *RSC Advances*, *10*(41), 24215-24233. https://doi.org/10.1039/d0ra04851h

Jiménez-Calvo, P., Caps, V., & Keller, V. (2021). Plasmonic Au-based junctions onto TiO$_2$, gC$_3$N$_4$, and TiO$_2$-gC$_3$N$_4$ systems for photocatalytic hydrogen production: Fundamentals and challenges. *Renewable and Sustainable Energy Reviews*, *149*, 111095. https://doi.org/10.1016/j.rser.2021.111095

Jorfi, S. (2018). Visible light photocatalytic degradation of Azo dye and a real textile wastewater using Mn, Mo, La/ TiO$_2$/AC nanocomposite. *Chemical and Biochemical Engineering Quarterly*, *32*(2), 215-227. https://doi.org/10.15255/cabeq.2017.1261

Kiwaan, H., Atwee, T., Azab, E., & El-Bindary, A. (2019). Photocatalytic degradation of organic dyes in the presence of nanostructured titanium dioxide. *Journal of Molecular Structure*, *1200*, 127115. https://doi.org/10.1016/j.molstruc.2019.127115

Lee, H., Jang, H. S., Kim, N. Y., & Joo, J. B. (2021). Cu-doped TiO$_2$ hollow nanostructures for the enhanced photocatalysis under visible light conditions. *Journal of Industrial and Engineering Chemistry*, *99*, 352-363. https://doi.org/10.1016/j.jiec.2021.04.045

Lellis, B., Fávaro-Polonio, C. Z., Pamphile, J. A., & Polonio, J. C. (2019). Effects of textile dyes on health and the environment and bioremediation potential of living organisms. *Biotechnology Research and Innovation*, *3*(2), 275-290. https://doi.org/10.1016/j.biori.2019.09.001

Li, N., Geng, D., & Zhou, J. (2021). Ag and Cu Nanoparticles Synergistically Enhance Photocatalytic CO2 Reduction Activity of B Phase TiO$_2$. *Catalysis Letters*, *152*(1), 124-138. https://doi.org/10.1007/s10562-021-03618-4

Mao, T., Zha, J., Hu, Y., Chen, Q., Zhang, J., & Luo, X. (2024). Research progress of TiO$_2$ modification and

photodegradation of organic pollutants. *Inorganics*, *12*(7), 178. https://doi.org/10.3390/inorganics12070178

Mapukata, S., Shingange, K., & Mokhena, T. (2023). Review of the recent advances on the fabrication, modification and application of electrospun TiO_2 and ZnO nanofibers for the treatment of organic pollutants in wastewater. *Frontiers in Chemical Engineering*, *5*. https://doi.org/10.3389/fceng.2023.1304128

Mortazavian, S., Saber, A., & James, D. E. (2019). Optimization of Photocatalytic Degradation of Acid Blue 113 and Acid Red 88 Textile Dyes in a UV-C/TiO2 Suspension System: Application of Response Surface Methodology (RSM). Catalysts, 9(4), 360. https://doi.org/10.3390/catal9040360

Mustapha AM, Ameuru US, Giwa A, Danladi E (2025) Synthesis, characterisation, and dyeing performance of novel naphthalimide-based monoazo acid dyes on nylon 6.6 fabrics. *UMYU Scientifica,* *4*(2), 457 - 474. https://doi.org/10.56919/usci.2542.048

Olya, M., Vafaee, M., & Jahangiri, M. (2015). Modeling of acid dye decolorization by TiO_2-Ag_2O nano-photocatalytic process using response surface methodology. *Journal of Saudi Chemical Society*, *21*(6), 633-642. https://doi.org/10.1016/j.jscs.2015.07.006

Rajesh, C., Rajashekara, R., & Nagaraju, P. (2023). Response Surface Methodology (RSM) modelling for the photocatalytic optimization study of benzophenone removal using $CuWO_4$/NiO nanocomposite. *Journal of Environmental Health Science and Engineering*, *21*(1), 187-199. https://doi.org/10.1007/s40201-023-00852-3

Reza, K. M., Kurny, A., & Gulshan, F. (2015). Parameters affecting the photocatalytic degradation of dyes using TiO_2: a review. *Applied Water Science*, *7*(4), 1569-1578. https://doi.org/10.1007/s13201-015-0367-y

Saba, A. I., & Elsheikh, A. H. (2020). Forecasting the prevalence of COVID-19 outbreak in Egypt using nonlinear autoregressive artificial neural networks. *Process Safety and Environmental Protection*, *141*, 1-8. https://doi.org/10.1016/j.psep.2020.05.029

Saleh, I. A., Zouari, N., & Al-Ghouti, M. A. (2020). Removal of pesticides from water and wastewater: Chemical, physical and biological treatment approaches. *Environmental Technology & Innovation*, *19*, 101026. https://doi.org/10.1016/j.eti.2020.101026

Sapcharoenkun, C., Kanpairee, P., Phaitakeaw, P., Punklahan, N., Butburee, T., Sangkhun, W., Treetong, A., Theanngern, K., Muensri, P., Wutikhun, T., Tanthanuch, W., Teeravechyan, S., Sae-Ueng, U., Kangwansupamonkon, W., Supcharoengoon, U., Leeladee, P., & Eksangsri, T. (2025). Synergistic Enhancement of Photocatalytic Oxidation in Wastewater Treatment using Cu/Ag Co-doped TiO_2 Nanoparticles. *Journal of Alloys and Compounds*, *1036*, 181788. https://doi.org/10.1016/j.jallcom.2025.181788

Shaki, H., Khosravi, A., & Gharanjig, K. (2017). Novel self-coloured polymers based on new fluorescent naphthalimide derivatives: synthesis, characterisation and photophysical properties. *Pigment & Resin Technology*, *46*(3), 244-250. https://doi.org/10.1108/prt-07-2016-0080

Shi, Z., Song, Q., Göstl, R., & Herrmann, A. (2021). The Mechanochemical Release of Naphthalimide Fluorophores from β-Carbonate and β-Carbamate Disulfide-Centered Polymers. *CCS Chemistry*, *3*(11), 2333-2344. https://doi.org/10.31635/ccschem.021.202101147

Slamet, N., Nasution, H. W., Purnama, E., Kosela, S., & Gunlazuardi, J. (2005). Photocatalytic reduction of CO_2 on copper-doped Titania catalysts prepared by improved-impregnation method. *Catalysis Communications*, *6*(5), 313-319. https://doi.org/10.1016/j.catcom.2005.01.011

Swaminaathan, P., Saravanan, A., Yaashikaa, P., & Vickram, A. (2024). Recent advances in photocatalytic degradation of persistent organic pollutants: Mechanisms, challenges, and modification strategies. *Sustainable Chemistry for the Environment*, *8*, 100171. https://doi.org/10.1016/j.scenv.2024.100171

Tolosana-Moranchel, A., Pecharromán, C., Faraldos, M., & Bahamonde, A. (2020). Strong effect of light scattering by distribution of TiO_2 particle aggregates on photocatalytic efficiency in aqueous suspensions. Chemical Engineering Journal, 403, 126186. https://doi.org/10.1016/j.cej.2020.126186

Tran, H. D., Nguyen, D. Q., T, P., DO, & Tran, U. N. P. (2023). Kinetics of photocatalytic degradation of organic compounds: a mini-review and new approach. RSC Advances, 13(25), 16915–16925. https://doi.org/10.1039/d3ra01970e

Vaiano, V., & De Marco, I. (2023). Removal of Azo Dyes from Wastewater through Heterogeneous Photocatalysis and Supercritical Water Oxidation. *Separations*, *10*(4), 230. https://doi.org/10.3390/separations10040230

Vishani, D. B., & Shrivastav, A. (2021). Enzymatic decolorization and degradation of azo dyes. In *Elsevier eBooks* (pp. 419-432). https://doi.org/10.1016/b978-0-323-85657-7.00020-1

Yahya, N. A. A., Samir, O. M., Al-Ariki, S., Ahmed, A. a. M., & Swillam, M. A. (2023). Synthesis of novel antibacterial nanocomposite CuO/Ag-modified zeolite for removal of MB dye. *Scientific Reports*, *13*(1). https://doi.org/10.1038/s41598-023-40790-6

Zou, H., & Wang, Y. (2017). Azo dyes wastewater treatment and simultaneous electricity generation in a novel process of electrolysis cell combined with microbial fuel cell. *Bioresource Technology*, *235*, 167-175. https://doi.org/10.1016/j.biortech.2017.03.093